Vibrational analysis of HOCl up to 98% of the dissociation energy with a Fermi resonance Hamiltonian

Remy Jost[a)]
Grenoble High Magnetic Field Laboratory, MPI-FKF and CNRS, BP 166, F-38042 Grenoble Cedex 09, France

Marc Joyeux
Laboratoire de Spectrométrie Physique, CNRS UMR 5588, Université Joseph Fourier-Grenoble I, BP 87, F-38402 St Martin d'Hères Cedex, France

Sergei Skokov and Joel Bowman
Department of Chemistry and Cherry L. Emerson Center for Scientific Computation, Emory University, Atlanta, Georgia 30322

(Received 3 May 1999; accepted 15 June 1999)

We have analyzed the vibrational energies and wave functions of HOCl obtained from previous *ab initio* calculations [J. Chem. Phys. **109**, 2662 (1998); **109**, 10273 (1998)]. Up to approximately 13 000 cm^{-1}, the normal modes are nearly decoupled, so that the analysis is straightforward with a Dunham model. In contrast, above 13 000 cm^{-1} the Dunham model is no longer valid for the levels with no quanta in the OH stretch ($v_1=0$). In addition to v_1, these levels can only be assigned a so-called polyad quantum number $P=2v_2+v_3$, where 2 and 3 denote, respectively, the bending and OCl stretching normal modes. In contrast, the levels with $v_1 \geqslant 2$ remain assignable with three v_i quantum numbers up to the dissociation ($D_0=19\,290\ cm^{-1}$). The interaction between the bending and the OCl stretch ($\omega_2 \cong 2\omega_3$) is well described with a simple, fitted Fermi resonance Hamiltonian. The energies and wave functions of this model Hamiltonian are compared with those obtained from *ab initio* calculations, which in turn enables the assignment of many additional *ab initio* vibrational levels. Globally, among the 809 bound levels calculated below dissociation, 790 have been assigned, the lowest unassigned level, No. 736, being located at 18 885 cm^{-1} above the (0,0,0) ground level, that is, at about 98% of D_0. In addition, 84 ''resonances'' located above D_0 have also been assigned. Our best Fermi resonance Hamiltonian has 29 parameters fitted with 725 *ab initio* levels, the rms deviation being of 5.3 cm^{-1}. This set of 725 fitted levels includes the full set of levels up to No. 702 at 18 650 cm^{-1}. The *ab initio* levels, which are assigned but not included in the fit, are reasonably predicted by the model Hamiltonian, but with a typical error of the order of 20 cm^{-1}. The classical analysis of the periodic orbits of this Hamiltonian shows that two bifurcations occur at 13 135 and 14 059 cm^{-1} for levels with $v_1=0$. Above each of these bifurcations two new families of periodic orbits are created. The quantum counterpart of periodic orbits are wave functions with ''pearls'' aligned along the classical periodic orbits. The complicated sequence of *ab initio* wave functions observed within each polyad is nicely reproduced by the wave functions of the Fermi resonance Hamiltonian and by the corresponding shapes of periodic orbits. We also present a comparison between calculated and measured energies and rotational constants for 25 levels, leading to a secure vibrational assignment for these levels. The largest difference between experimental and calculated energies reaches 22 cm^{-1} close to D_0. © *1999 American Institute of Physics.* [S0021-9606(99)01034-X]

I. INTRODUCTION

The HOCl molecule plays an important role in the chemistry of the upper atmosphere as a reservoir of OH and chlorine.[1] Its phodissociation, either into OH and Cl, or HCl and O, or H and OCl gives reactive species of atmospheric relevance.[2] HOCl has been first studied by visible[3] and IR[4–9] absorption. Recently, the highly excited vibrational levels of HOCl have been studied in four related projects: (a) the 3–5 overtones of the OH stretch have been observed and analyzed using intracavity absorption (ICLAS);[10–12] (b) eigenstate selected unimolecular dissociation rates have been measured close to the dissociation threshold;[13–15] (c) dissociation rates have been calculated;[16,17] and (d) an *ab initio* potential energy surface (PES), including the corresponding vibrational eigenstates, has been calculated up to and above dissociation.[18–20] The spectroscopic (energies, wave functions) and dynamic aspects being strongly linked, both below the dissociation threshold (IVR mechanisms) and above it (dissociation rates), it was tempting to extract, from the *ab initio* results, some relevant information for the interpretation of the experimental results mentioned above.

Recently, potential energy surfaces (PESs) for other triatomics like H_2O, HCN/HNC, HO_2, HCP, H_3^+, and NO_2 have been calculated up to and above the dissociation and/or

a)Electronic mail: jost@polycnrs-gre.fr

isomerization energies. These surfaces have been used in exact calculations of vibrational energies and wave functions. Such calculations are numerically intensive and the results are not always easily understood. A complimentary and computationally less expensive approach to understanding and interpreting vibrational spectra is provided by constructing an effective Hamiltonian. The goal of this paper is to analyze the vibrational energies of HOCl and to describe, with a simple and compact effective Hamiltonian, the ground electronic state of HOCl. Our results show that the dominant features of its intramolecular dynamics are well reproduced by this effective Hamiltonian which is obtained from a detailed analysis of the *full* set of calculated vibrational eigenstates (energies and wave functions), which includes 809 bound levels below dissociation [$D_0 = 19\,920\ \mathrm{cm}^{-1}$ (Refs. 13–15)]. At this point, it should be mentioned that only 25 vibrational levels have been experimentally observed, with most having excitation in the OH stretch. In contrast, less information concerning the two other modes (the bending and the OCl stretch) is experimentally accessible. The main advantage of the *ab initio* methods (compared to the experimental approach) is that calculations of all the levels can be done, thereby gaining a global description of the spectroscopic and dynamic properties of each molecule, even if the precision of the energies is significantly below that of experiment. The main feature of the ground state of HOCl is the regular behavior of the vibrational energy levels, which can be deduced from the statistical analysis of levels spacing distributions.[19] This is due to the near separability of the three normal modes. Indeed, the inspection of the equipotential energy plots (see Fig. 4 in Ref. 18) suggests only moderate coupling of the OCl and OH stretches with the bending mode. Far above the dissociation threshold, the OH stretch and the bend become strongly coupled, due to the HOCl→HClO isomerization. However, here we are only concerned with vibrational states up to the OH+Cl dissociation energy at 19 290 cm^{-1} and the potential used does not contain this isomer (the newer potential of Ref. 20 does contain the isomer).

One goal of the present work is to determine up to which energy the assignment of these calculated vibrational states is possible. Surprisingly, the assignment was possible almost up to dissociation and, for many levels (resonances), even above dissociation. In addition the observed pattern of vibrational energies and wave functions can be interpreted, in the framework of semiclassical analysis, in terms of bifurcation(s) and periodic orbits.[21–33] This results in a condensation of the huge amount of data provided by *ab initio* calculations by a simple and compact analytic Hamiltonian, for which the semiclassical analysis reproduces the dominant features of the spectroscopic and dynamic vibrational properties of HOCl up to and even above dissociation. This paper is organized as follows: The *ab initio* results are summarized in Sec. II. In Sec. III, we present the Dunham analysis, which shows that above 13 000 cm^{-1} the O–Cl stretch interacts strongly with the bending mode. Section IV is devoted to the description of the fitted Fermi resonance Hamiltonian, which describes the complete set of HOCl vibrational energies up to 18 885 cm^{-1}, i.e., 98% of the dissociation energy. Section V contains the semiclassical analysis of the Fermi resonance Hamiltonian and shows the bifurcations and the corresponding new families of periodic orbits. In Sec. VI, the *ab initio* vibrational energies and rotational constants are compared to the existing experimental values.

II. *AB INITIO* CALCULATIONS, POTENTIAL ENERGY SURFACE, AND VIBRATIONAL ENERGIES

The *ab initio* calculations for HOCl, fitting of the PES, and variational calculations of vibrational states have been presented in previous papers[16,18–20] and are only summarized here. The *ab initio* calculations were performed by Peterson for 756 HOCl geometries employing the correlation-consistent double, triple, and quadruple basis sets of Dunning and co-workers,[34,35] the electron correlation effects being incorporated by using internally contracted multireference configuration interaction (icMRCl) wave functions.[36,37] The results of *ab initio* calculations were extrapolated to the complete basis set limit and then used for the fit of the PES. The one-dimensional (1D) OH diatomic potentials were fitted by Morse-type functions for a set of fixed values of the two other coordinates, namely the OCl distance and the HOCl angle, and then a three-dimensional (3D) surface was obtained as a two-dimensional (2D) spline of Morse parameters over the ranges of the OCl distance and HOCl angle. The splines were arbitrarily truncated at an OCl distance equal to $10a_0$ and, beyond this distance, energy was assumed to depend only on the OH bond length. Based on preliminary calculations, the PES was adjusted to improve the agreement with experimental data.[18] In particular, the PES minimum was shifted to the exact experimental geometry, dissociation energy was adjusted, and coordinates slightly rescaled. After these adjustments, the HOCl experimental vibrational energies up to six quanta in the OH stretch were reproduced to within a few cm^{-1}.[19] Excellent agreement with experiment was also found for a number of rotational and rovibrational energies of bound,[18] as well as resonance states.[20] The HOCl dissociation energy is computed at 19 289.2 cm^{-1}, in good agreement with the experimental value of 19 289.6 cm^{-1}.[13,15]

The $J=0$ vibrational eigenstates and eigenfunctions analyzed here were computed[16] using the truncation/recoupling method.[19] The calculations were performed in Jacobi coordinates R, r, and γ, where R is the distance from Cl to G, the center of mass of OH, r is the OH bond length, and γ the OGCl angle set to 0 at linear HOCl geometry. After a series of truncations of reference 1D and 2D Hamiltonians, the size of the final 3D Hamiltonian matrix was reduced to 7200, which is small enough to be diagonalized directly by standard diagonalization routines. The details of the truncation/recoupling method and of more specific details of the calculations, such as basis sets, grids, etc., can be found in Refs. 19 and 16, respectively.

Due to the relatively small size of the basis set, all the necessary eigenfunctions could be stored in memory or on disk for further use. In particular, the eigenfunctions were used to compute expectation values for the Jacobi coordinates for the first 1500 wave functions. Note that, due to the large mass of Cl, the Jacobi distance R is very close to the

OCl bond length and therefore the expectation value for R is a good indicator of the OCl bond stretching excitation in each eigenstate.

III. VIBRATIONAL ANALYSIS USING A DUNHAM EXPANSION

Only the $HO^{35}Cl$ isotope will be discussed in this article. However, most of the results are expected to remain valid for the $HO^{37}Cl$ isotope.

Having in hand the calculated vibrational energies as well as the associated wave functions and expectation values, one can try to assign quantum numbers to these levels. The shape of the PES (see Fig. 4 of Ref. 18) indicates that the normal modes 1–3 should be close, respectively, to r (OH stretch), γ (bending), and R (close to the O–Cl stretch), the Jacobi coordinates used in Ref. 18. The approximate 1:2 frequency ratio between the O–Cl stretch and the bending plays a crucial role in the vibrational assignment. In contrast, the 1:3 ratio between the bending and the O–H stretch plays only a minor role in the vibrational analysis, because it induces only the local interactions briefly discussed below.

After a straightforward vibrational assignment of about 100 levels with three quantum numbers v_1, v_2, v_3, a preliminary Dunham fit, including typically 20 parameters [see Eq. (2) in Sec. IV], was performed on these levels, with a rms of a few cm^{-1} (much less than the average spacing). Based on the predictions given by this Dunham model, a large number of higher levels could be assigned easily. In fact, the 3D (v_1, v_2, v_3) vibrational analysis (i.e., the assignment procedure) can easily be split into one 2D analysis involving only v_2 and v_3 for each value of the OH stretching quantum number, v_1. Indeed, the v_1 assignment is straightforward, because of the regular evolution of the expectation values calculated for each eigenstate. Around and above 13 500 cm^{-1} [unless specified, the energies are given relative to the (0,0,0) ground state located at 2867.0 cm^{-1} above the bottom of the PES], it becomes obvious that the Dunham fit is no longer able to describe correctly the levels for which only the bending and the O–Cl stretch are excited, i.e., levels with $v_1 = 0$. The anharmonicity of the OCl stretch (described by the x_{33} and higher order terms in the Dunham fit) being significantly larger than that of the bending motion (parameters $x_{22}\cdots$), a crossover occurs between the bending and the O–Cl stretch progressions. The Fermi resonance which couples these two modes is then strong enough to destroy the v_2 and v_3 quantum numbers. This corresponds to a bifurcation in the semiclassical analysis presented in the following sections. These two quantum numbers are replaced by a single polyad quantum number, $P = 2v_2 + v_3$. The effect of this crossover can also be observed on the evolution of the expectation values which reflect the properties of the wave functions. In contrast, the levels with v_1 larger than zero remain easily assignable above 13 500 cm^{-1}. The crossovers in the progression of levels having $v_1 = 1$ occurs around 17 500 cm^{-1}. The crossover for the progressions with $v_1 \geqslant 2$ occurs above the dissociation energy. The energy range covered by each polyad is represented by a vertical line in Fig. 1. For the sake of clarity, the levels with different v_1 are shifted horizontally. The 32 fitted Dunham parameters ($3\omega_i$, $6x_{ij}$, $10y_{ijk}$ and $13z_{ijkl}$ parameters) given in Table I correspond to a set of 314 levels fitted with a rms error of 2.62 cm^{-1}. This set of 314 levels includes 75 levels with $v_1 = 0$ (upper level at 10 060 cm^{-1}), 70 levels with $v_1 = 1$ (upper level at 14 000 cm^{-1}), 73 levels with $v_1 = 2$ (upper level at

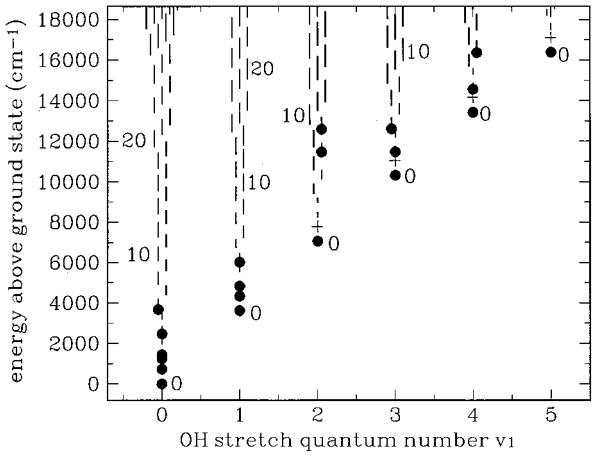

FIG. 1. Energy range classification of the HOCl vibrational levels sorted by polyads for each v_1 (OH stretch) family. Each vertical bar shows the energy range covered by the levels belonging to a given polyad P. Polyads 0, 10 and 20 are indicated as a P scale. The polyads are represented vs v_1 (OH stretch) along the horizontal axis in order to avoid too many overlaps. The closed dots correspond to the levels observed experimentally up to 18 000 cm^{-1} and listed in Table III.

TABLE I. Dunham parameters (in cm^{-1}). The uncertainty is given as plus or minus two times the standard deviation.

ω_1	3788.47	±4.328
ω_2	1245.09	±2.209
ω_3	739.685	±1.445
x_{11}	−84.540	+2.620
x_{22}	+2.181	±0.743
x_{33}	−3.517	±0.377
x_{12}	−16.291	±2.266
x_{13}	−0.490	±0.950
x_{23}	−7.049	±0.660
y_{111}	−0.173	±0.634
y_{222}	−0.778	±0.009
y_{333}	−0.259	±0.035
y_{112}	−0.154	±0.673
y_{122}	−3.965	±0.401
y_{113}	+0.508	±0.155
y_{133}	−0.122	±0.131
y_{223}	−0.428	±0.071
y_{233}	−0.131	±0.109
y_{123}	−0.767	±0.350
z_{1111}	+0.0153	±0.0506
z_{2222}	+0.0111	±0.0038
z_{3333}	+0.0098	±0.0011
z_{1112}	+0.0793	±0.0649
z_{1122}	−0.0426	±0.0044
z_{1133}	−0.0174	±0.0143
z_{1222}	+0.2885	±0.0246
z_{1333}	−0.0007	±0.0048
z_{2233}	−0.0079	±0.0084
z_{2333}	+0.0021	±0.0047
z_{1123}	−0.1553	±0.0426
z_{1223}	+0.1003	±0.0285
z_{1233}	+0.0854	±0.0177

17 100 cm^{-1}), 49 levels with $v_1=3$ (upper level at 18 130 cm^{-1}) and 32, 13, and 2 levels with $v_1=4$, 5, and 6, respectively, these levels lying up to about 19 900 cm^{-1}. This choice of 32 parameters is more or less arbitrary: all $6x_{ij}$ and the $10y_{ijk}$ parameters were kept, even when the error bar is larger than the parameter value. The 13 selected z_{ijkl} are those contributing to a reduction of the rms, but this choice, selected after numerous tries, remains more or less arbitrary. The upper energies given above for the $v_1=0-3$ sequences correspond roughly to the upper limit of validity for the Dunham expansion. Above these energies, the interaction (Fermi resonance) between the OCl stretch and the bending becomes important and the levels cannot be described any longer by a Dunham expansion.

In addition, it should be noted that the 1:3 resonance between the OH stretch and the bending modes is effective at energies as low as 6250 cm^{-1}, where the (1,1,2) level interacts with the (0,4,2) level (see Sec. IV). The energy shifts due to this interaction are typically less than 10 cm^{-1} and this stretch–bend interaction, which is large in other molecules, plays only a minor role in HOCl. However, some pairs of wave functions reveal unambiguously this interaction, as discussed in Sec. IV. Globally, the Dunham analysis allows us to assign at most about 350 levels including some levels up to and above the dissociation energy (see the list above). However, many levels, which cannot be assigned three quantum numbers can still be assigned a v_1 and a P (polyad, see above) quantum numbers. At this stage, it is necessary to consider an explicit form of the O–Cl stretch–bending interaction, i.e., the Fermi resonance, to quantitatively describe the *ab initio* vibrational energies. This is the purpose of Sec. IV.

IV. VIBRATIONAL ANALYSIS WITH A FERMI RESONANCE HAMILTONIAN

The Fermi resonance Hamiltonian is a polynomial expansion in terms of the normal mode coordinates and momenta (p_i,q_i), or alternately in terms of the corresponding creation and annihilation operators (a_i,a_i^+). The Hamiltonian can be split into three parts:

$$H=H_D+H_F+H_C, \tag{1}$$

where H_D is a Dunham expansion, H_F is the Fermi 1:2 nonlinear resonance between the bending (mode 2) and the OCl stretch (mode 3), and H_C is the additional 3:1 nonlinear resonance between the OH stretch (mode 1) and the bend (mode 2). The Dunham expansion is diagonal in the normal mode basis. The matrix elements are taken in the form:

$$\begin{aligned}\langle v_1,v_2,v_3|H_D|v_1,v_2,v_3\rangle &= \sum_i \omega_i n_i+\sum_{i\leqslant j} x_{ij}n_in_j+\sum_{i\leqslant j\leqslant k} y_{ijk}n_in_jn_k \\ &+\sum_{i\leqslant j\leqslant k\leqslant m} z_{ijkm}n_in_jn_kn_m \\ &+\sum_{i\leqslant j\leqslant k\leqslant m\leqslant n} z_{ijkmn}n_in_jn_kn_mn_n,\end{aligned} \tag{2}$$

where $n_i=v_i+1/2$. The Fermi interaction which couples the bending and the OCl stretching motion arises from terms like $q_2q_3^2$, $p_2p_3q_3$, and so on. However, in the effective Hamiltonian, only the terms of the form $(a_2a_3^+a_3^++a_2^+a_3a_3)$ are retained, because this is the only contribution which couples basis levels brought into close degeneracy by the approximate 1:2 ratio between ω_2 and ω_3. The additional matrix elements due to $q_2q_3^2$, $p_2p_3q_3$, and so on, couple energetically well separated basis levels, and canonical perturbation theory shows that they can safely be absorbed in the Dunham expansion. Therefore, the Fermi resonance matrix element is taken in the form:

$$\begin{aligned}\langle v_1,v_2,v_3|H_F|v_1,v_2-1,v_3+2\rangle &= \sqrt{v_2(v_3+1)(v_3+2)}\left(k+\sum_i k_in_i+\sum_{i\leqslant j}k_{ij}n_in_j\right),\end{aligned} \tag{3}$$

where $n_1=v_1+1/2$, $n_2=v_2$, and $n_3=v_3+3/2$ (these values for n_1, n_2, and n_3 in an off-diagonal matrix element are obtained from the simplest symmetrized arrangement of creation and annihilation operators, which is discussed, for example,in Sec. IV C of Ref. 38). Similarly, the additional 3:1 resonance between the OH stretch and bending motions is based on the single coupling term $(a_1a_2^+a_2^+a_2^++a_1^+a_2a_2a_2)$, and the corresponding matrix element is

$$\begin{aligned}\langle v_1,v_2,v_3|H_C|v_1-1,v_2+3,v_3\rangle &= K\sqrt{v_1(v_2+1)(v_2+2)(v_2+3)}.\end{aligned} \tag{4}$$

Note that v_1 and P are good quantum numbers for H_D+H_F, whereas there remains only one good quantum number for $H_D+H_F+H_C$, namely $3v_1+P$. However, since only a few pairs of levels are substantially coupled by H_C, approximate good quantum numbers v_1 and P can be assigned to all the levels of $H_D+H_F+H_C$, according, for example, to the procedure described in Sec. III D of Ref. 38.

The iterative fitting procedure used to determine the Fermi resonance Hamiltonian is analogous to the one used for the Dunham model. The crucial importance of the nonlinear resonances appears when considering the energy values, but most of all when the wave functions are also examined (see below). The results of numerical calculations will now be presented, and the results of exact quantum diagonalizations will then be interpreted in light of the polyad structure of the Fermi resonance Hamiltonian.

A total of 874 vibrational levels have been assigned, 790 below the dissociation threshold and 84 above it. The list of levels and their assignments can be sent upon request to the authors. The first unassigned level, No. 736, calculated at 18 885 cm^{-1} is located at about 98% of the dissociation energy ($D_0=19\,290\,cm^{-1}$). Among the 809 vibrational levels calculated up to D_0, only 19 remain unassigned. This means that it is possible to assign at least a v_1, a P, and a sequence number to 97.5% of the bound vibrational levels. All the unassigned levels should have $v_1=0$, because all the levels with $v_1\geqslant 1$ predicted below D_0 have been assigned. Furthermore, the Fermi resonance Hamiltonian shows that the unassigned levels should be low energy members of polyads with large values of P (typically $34<P<50$). It should be noted

TABLE II. Parameters of the Fermi resonance Hamiltonian (in cm^{-1}). The uncertainty is given as plus or minus two times the standard deviation.

ω_1	3777.067	±3.172
ω_2	1258.914	±1.368
ω_3	753.834	±0.564
x_{11}	−80.277	±1.126
x_{22}	−3.204	±0.174
x_{33}	−7.123	±0.036
x_{12}	−19.985	±1.108
x_{23}	−10.637	±0.282
y_{111}	−0.361 9	±0.113 2
y_{333}	+0.082 5	±0.000 6
y_{122}	−1.953 4	±0.280 0
y_{133}	−0.053 2	±0.010 0
y_{223}	−0.080 2	±0.016 8
y_{233}	−0.250 3	±0.022 0
z_{2222}	−0.041 17	±0.000 60
z_{3333}	−0.001 71	±0.000 02
z_{1122}	−0.150 70	±0.050 10
z_{1222}	+0.131 89	±0.017 92
z_{2333}	−0.012 29	±0.000 45
z_{1233}	+0.023 81	±0.008 70
z_{22222}	+0.001 51	±0.000 02
z_{22333}	−0.000 66	±0.000 02
k	0.000 00	(fixed)
k_2	−0.760 17	±0.063 47
k_3	−0.249 39	±0.005 913
k_{22}	−0.011 58	±0.002 138
k_{23}	+0.040 75	±0.004 977
k_{33}	+0.005 83	±0.000 247
K	+0.195 20	±0.100 16

that these levels, which span the O–Cl dissociation channel, may only roughly be described by the present PES since the OCl energy dependence was truncated at an OCl distance equal to $10a_0$.[18] (A new global analytical PES has been recently developed[39] which represents more accurately the long range tail of the HO–Cl interaction and thus will allow a more accurate description of highly excited OCl states.) In addition, 84 levels located above D_0 and up to 21 716 cm^{-1} could also be unambiguously assigned. These are the resonance states with typically very narrow widths.[16] Among these 874 assigned vibrational levels, only 725 have been included in the fit of the Fermi resonance Hamiltonian, because more and more accidental couplings are observed between neighboring levels which cannot be reproduced using the Hamiltonian in Eqs. (1)–(4). The lowest level not included in the fit is No. 703 at about 18 650 cm^{-1}, whereas the higher lying levels taken into account have $v_1 \geqslant 1$ and are therefore not much perturbed by the dissociation. Included in the fit are levels with up to 38 quanta in the O–Cl stretching motion ($P \leqslant 38$) and 7 quanta in the O–H stretching motion ($v_1 \leqslant 7$). The polyads are complete up to $[v_1,P]=[0,31]$, [1,25], [2,20], [3,13], [4,8], [5,4], [6,2], and [7,0]. The 725 selected levels were fitted with a total of 29 parameters, which are listed in Table II. The rms error is 5.29 cm^{-1} and the maximum error is 27.08 cm^{-1}. Upon neglect of the 3:1 resonance between modes 1 and 2, that is when putting $K=0$ in Eq. (4), the rms error rises only up to 5.33 cm^{-1}, which means that H_C is statistically of little consequence for the calculation of energy values. However, the agreement between the *ab initio* PES and the Fermi resonance Hamiltonian is substantially improved for about 15 pairs of levels, especially for wave functions, when H_C is taken into account. For example, the lowest pair of levels strongly coupled by H_C are Nos. 39 and 40 at about 6250 cm^{-1} above the ground state, and H_C is here necessary to reproduce the strong mixing observed in the wave functions. But once again, H_C is responsible only for local interactions and does not substantially influence either the global structure of the HOCl vibrational eigenstates at high energy values or the classical phase space structure. Therefore, in the further analysis, the 3:1 resonance between the OH stretch and the bend will simply be ignored.

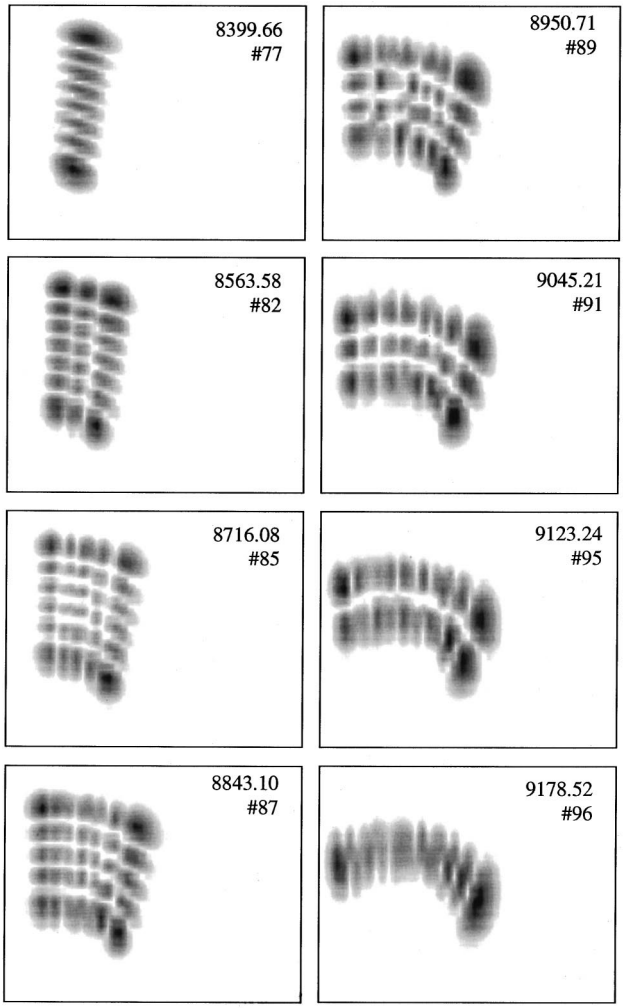

FIG. 2. *Ab initio* wave functions of the vibrational levels belonging to polyad $[v_1,P]=[0,14]$. The horizontal axis is the R Jacobi coordinate ($2.65<R<5.3$) and the vertical axis $\cos(\gamma)(-1<\cos\gamma<+1)$. The lowest level in this polyad (No. 77) can be assigned as (0,7,0) (pure bending), the second one (No. 82) as (0,6,2), and so on up to level 96 which is the (0,0,14) pure O–Cl stretch. Note that the number of nodes along the OCl stretch is not easy to count for the four higher levels of this polyad because the normal coordinates are not exactly the Jacobi r, R and γ coordinates. The energy (cm^{-1}) and the rank (#) are given for each level.

The wave function of the eight levels belonging to the polyad $[v_1,P]=[0,14]$ are plotted in Fig. 2 in order to show the regular evolution of the nodal structure of these wave functions in terms of the OCl stretch (the horizontal axis is the R Jacobi coordinate) and the bending angle (the vertical axis is the cosine of γ). This regularity explains the straight-

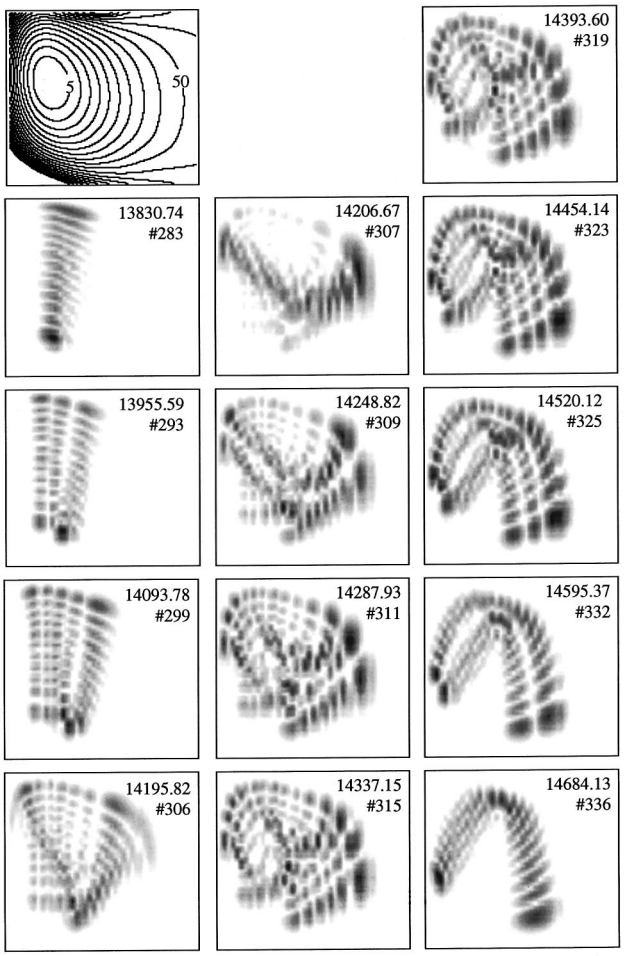

FIG. 3. *Ab initio* wave functions of the vibrational levels belonging to polyad $[v_1,P]=[0,24]$. The coordinates and scales are the same as in Fig. 2. The upper left panel gives the 2D plot of the PES. The lowest level (No. 283) can be assigned as (0,12,0) (pure bending), the second one (No. 293) as (0,11,2), the third one (No. 299) as (0,10,4), but the fourth one (No. 306) can hardly be assigned as (0,9,6). The fifth one (No. 307) resembles an almost pure OCl stretch. The highest members of this polyad converge toward level 336, which displays the ''horse-shoe'' $\cap$-shape due to the progressive transformation of the [*R*] periodic orbit (see Fig. 6). The energy (cm^{-1}) and the rank are given for each level.

forward assignments in terms of v_2 and v_3. In contrast, the family of wave functions of polyad $[v_1,P]=[0,24]$ presented in Fig. 3 shows that a new, $\cup$-shaped family of wave functions is created in addition to the bending and the OCl stretch families observed at lower energies, the latter having smoothly evolved to a ''horse-shoe,'' $\cap$-like shape. This new $\cup$-like type, which appears progressively starting from $P=18$, is clearly seen in all the polyads located above $P=24$. This can be checked in Fig. 4, where the complete set of wave functions for polyad $[v_1,P]=[0,30]$ is shown. This series of wave functions demonstrates that a dramatic change has occurred in the description of the eigenstates. The simplest way to rationalize these observations is to consider the semiclassical approach in which periodic orbits and bifurcations enable a classification of the quantum eigenstates. Indeed, following the pioneering work of Gutzwiller[21–23] and Heller,[24,25] there have been several numerical applications, which have demonstrated the importance of POs in understanding the localization of quantum wave functions, which in turn is helpful in understanding spectral patterns.[26–29] Recently, it has been shown for HCP that the drastic changes observed in the quantum wave functions around 13 000 cm^{-1} (i.e., polyad $P=18$), could be interpreted qualitatively in terms of POs and bifurcations.[30–33]

For the sake of comparison, the wave functions plotted in the (q_3,q_2) plane for the 16 levels of polyad $[v_1,P]=[0,30]$ obtained using the Fermi resonance Hamiltonian are displayed in Fig. 5. The periodic orbits are superimposed as discussed in Sec. V. This polyad, which ranges from 16 581 to 17 785 cm^{-1} above the ground state, is the next to last to be complete in our assignments for $v_1=0$. Figures 4 and 5 can be readily compared, because the two sets of coordinates, namely (R,γ) and (q_3,q_2) are close, despite the fact that they are not expressed in the same units. It should be noted, however, that the plots in the (q_3,q_2) plane are symmetric with respect to the $q_3=0$ axis, whereas the plots in the (R,γ) plane are not symmetric with respect to the equilibrium value for *R*. This reflects the nonlinear relationships between the Jacobi and normal coordinates. Keeping this point in mind, it is seen that the agreement between the nodal structure of these two sets of wave functions is good. In particular, the alternation of bending and stretching wave functions at the bottom of the polyad and then the progressive switching to a ''horse shoe'' ($\cap$-like) wave function are closely reproduced. Clearly, three v_i quantum numbers cannot be assigned to each level of this polyad. The remainder of this section, as well as Sec. V devoted to the semiclassical analysis of the Fermi resonance Hamiltonian, are aimed at understanding what happens in the energy gap between these two polyads. Polyads with $v_1=0$ will mainly be discussed, because levels with $v_1\geqslant 1$ are much less influenced by the Fermi resonance below the dissociation threshold.

The first point to be noted is that at ''low'' energy values (approximately up to polyad $P=20$), the polyads are very regular. The lowest energy level in the polyad has an almost pure bending wave function, whereas the highest energy level has an almost pure OCl stretching wave function. One goes from the low energy end to the high energy end of the polyad by withdrawing one node along the γ axis, while adding two of them along the *R* axis. As long as the neglect of the Fermi resonance H_F and the Dunham expansion of Sec. III is valid (approximately up to polyad $P=15$), the ''necklaces'' supporting the ''pearls'' of the wave functions remain rigorously parallel to the γ and *R* axes (see, e.g., Fig. 3 for polyad $P=14$). Starting with $P=15$, the ''necklace'' lying originally along the *R* axis acquires more and more bending character but the wave functions elongated along this necklace remain the highest energy ones in each polyad. For the highest energy polyads studied, the bending contribution is even larger than the OCl stretching contribution, leading to the pronounced ''horse-shoe'' ($\cap$-type) shape. This series of wave functions, which corresponds to the highest energy level in each polyad, can be easily followed up to very high energy values, and is shown in the third column of Fig. 6. *As a result, the highest energy wave function in each polyad, which at low P values points along the* OCl stretch, *andwhich is expected to converge to the*

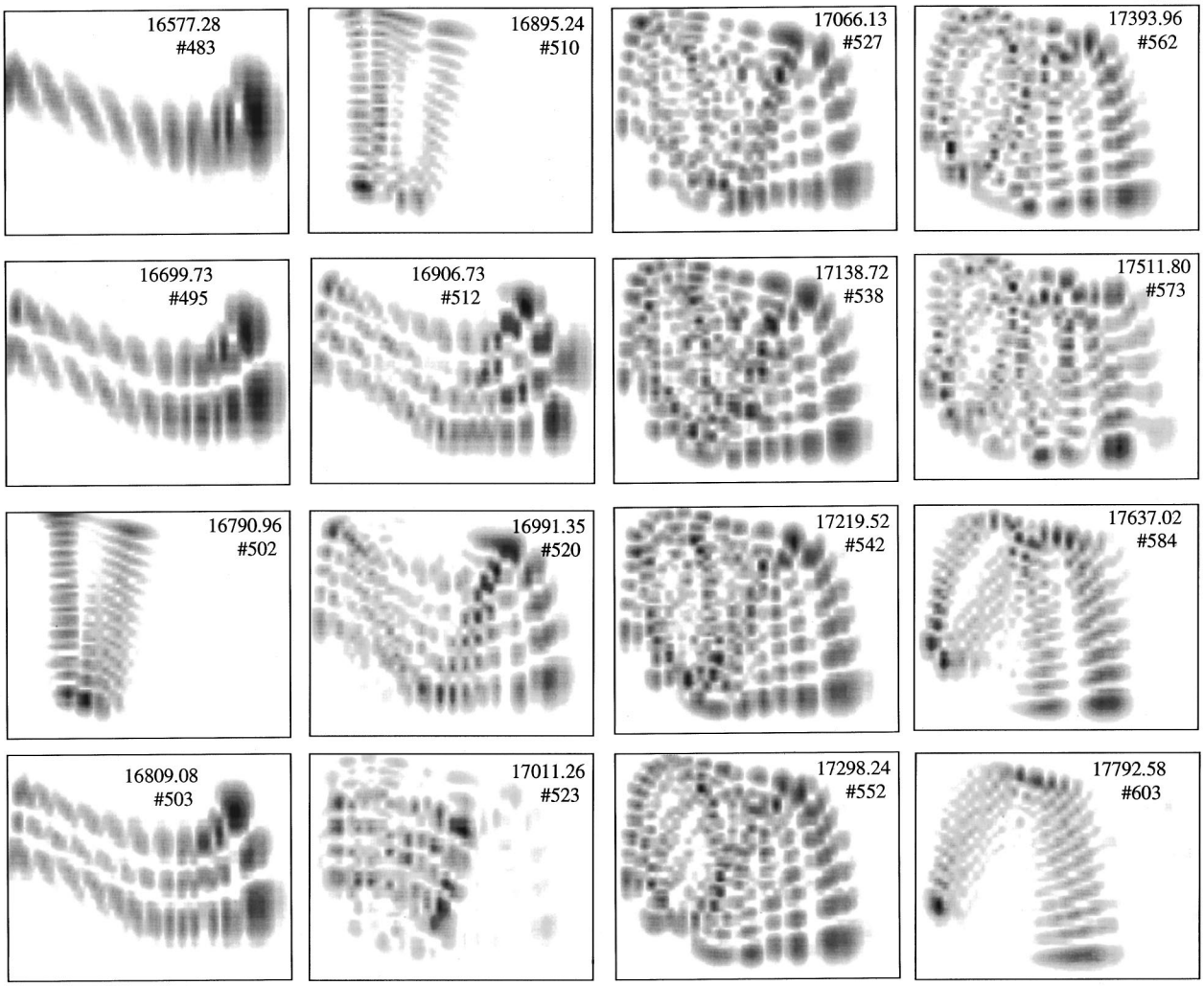

FIG. 4. *Ab initio* wave functions of the vibrational levels belonging to polyad $[v_1,P]=[0,30]$. The coordinates and scales are the same as in Figs. 2 and 3. The lowest level (No. 483) can be assigned as (0,0,30) (pure OCl stretch), the next one (No. 495) as (0,1,28), but the third one (No. 502) is mostly a bending level associated with the new stable periodic orbit [B2] discussed in Sec. V. The fourth level (No. 503) can be assigned as (0,2,26) but the fifth one (No. 510) has again many quanta in the bending mode and is again associated with the [B2] periodic orbit. The sixth level (No. 512) resembles the (0,3,24) state and the higher members of this polyad converge toward level 603, which displays the ''horse-shoe'' $\cap$-shape due to the progressive transformation of the [R] periodic orbit (see Fig. 6). The energy (cm^{-1}) and the rank (#) are given for each level.

HOCl→HO+Cl *dissociation pathway, progressively avoids this pathway*. This result is similar to the case of the HCP molecule[40–43] (where the original pure *bending* wave functions are observed to progressively avoid the isomerization pathway), except that the OCl stretch here plays the role assumed by the bending degree of freedom in HCP.

However, pure OCl stretching wave functions have not definitely disappeared. They instead reappear approximately in polyad $P=24$—but this time *in the middle* of the polyad—and progressively move to the *low energy end* of the polyad: e.g., the pure OCl stretching wave function is the fifth one (by increasing energy) in polyad $P=24$ and is the lowest one above $P=30$. This in part reflects the fact that, because of the anharmonicities, the energies of pure OCl stretching states are now below those of pure bending states. A smooth transition with coupled wave functions is observed between, say, polyads $P=20$ and $P=24$, but this new series of wave functions can then be followed again very clearly up to very high energy values, as can be checked in the second column of Fig. 6. This time, as far as can be understood from the comparison with the wave functions of the Fermi resonance Hamiltonian, this new family of wave functions appears *not to avoid* the dissociation pathway, at least up to 98% of the dissociation energy.

The fate of the pure bending wave functions is simpler, though not trivial: Indeed, the OCl stretching contribution to these wave functions remains small for the totality of the studied energy range. Moreover, as already stated, these wave functions are the lowest energy ones in each polyad up to $P=29$ and then move regularly toward the top of the polyad. But, at the same time, starting with $P=26$ or so, these wave functions progressively split into two branches and acquire a narrow V shape. This is clearly seen in the first column of Fig. 6.

How these quantum observations can be related to the classical dynamics of the system is the subject of Sec. V.

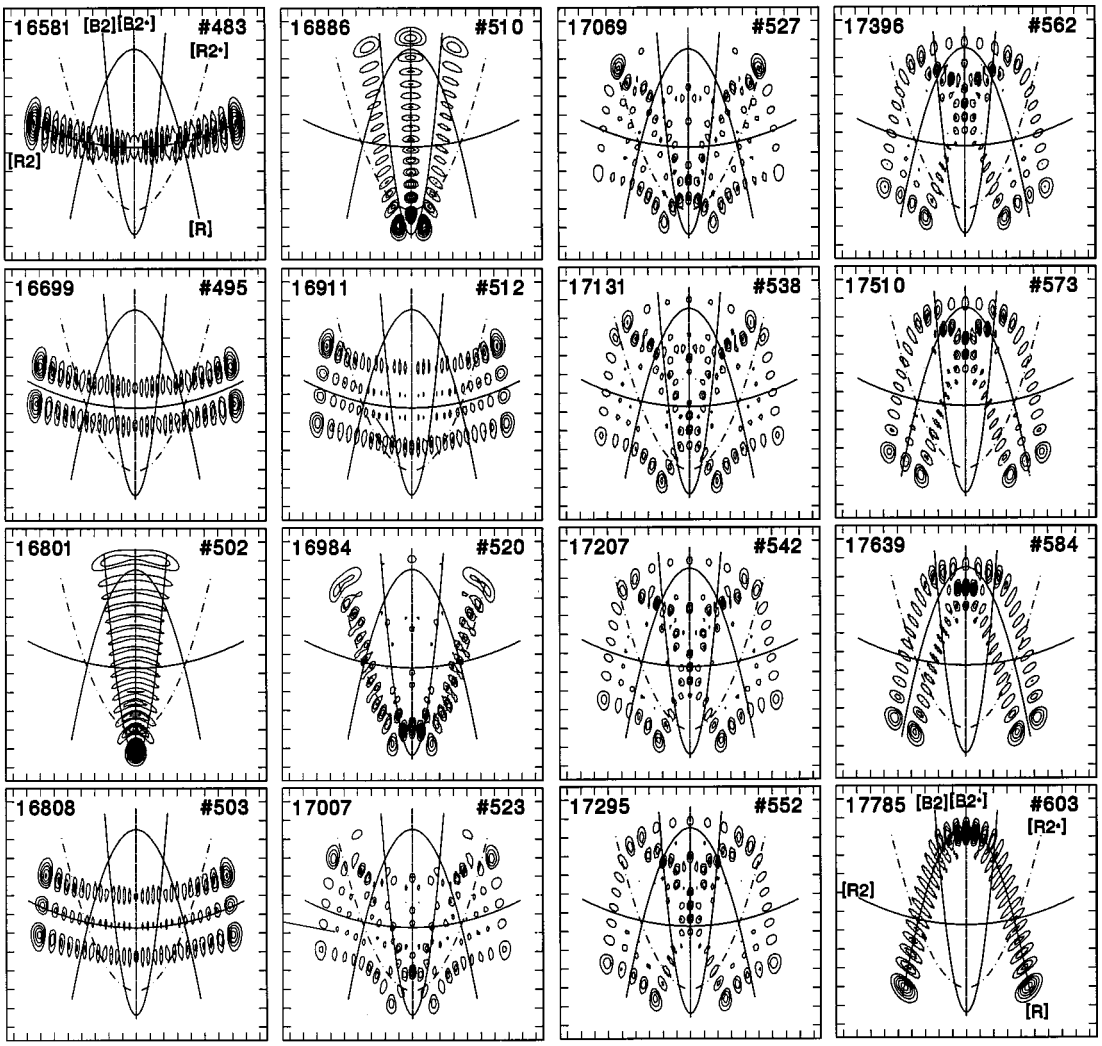

FIG. 5. Wave functions of the levels of polyad $[v_1,P]=[0,30]$ calculated with the Fermi resonance Hamiltonian. The horizontal and vertical axis are the OCl stretch ($-9.5<q_3<+9.5$) and bending ($-6.7<q_2<+6.7$) dimensionless normal coordinates of the Fermi resonance Hamiltonian. These normal mode coordinates are roughly similar to the axes in Figs. 2–4. The visual comparison of the nodal structure of the wave functions in Figs. 4 and 5 shows that there exists a one to one correspondence between these wave functions and that the Fermi resonance Hamiltonian reproduces well the complex progression of the *ab initio* vibrational eigenstates (energy and wave functions). The periodic orbits (POs) are superimposed to show the good correspondence between quantum and semiclassical analysis. The energy (cm^{-1}) and the rank (#) are given for each level.

V. SEMICLASSICAL ANALYSIS OF THE FERMI RESONANCE HAMILTONIAN

The expression of the classical Fermi resonance Hamiltonian is similar to the quantum one, except that p_i and q_i no longer denote quantum operators, but rather classical coordinates. Making the canonical transformation to zero-order action angle-like conjugate coordinates (I_i,φ_i), such that

$$q_i=\sqrt{2I_i}\cos\varphi_i, \quad p_i=-\sqrt{2I_i}\sin\varphi_i, \tag{5}$$

one obtains the following form for the classical Fermi resonance Hamiltonian:

$$H=H_D+H_F,$$

$$H_D=\sum_i \omega_i I_i+\sum_{i\leqslant j} x_{ij}I_iI_j + \sum_{i\leqslant j\leqslant k} y_{ijk}I_iI_jI_k \sum_{i\leqslant j\leqslant k\leqslant m} z_{ijkm}I_iI_jI_kI_m + \sum_{i\leqslant j\leqslant k\leqslant m\leqslant n} z_{ijkmn}I_iI_jI_kI_mI_n, \tag{6}$$

$$H_F=2I_2^{1/2}I_3\cos(\varphi_2-2\varphi_3)\left(k+\sum_i k_in_i+\sum_{i\leqslant j} k_{ij}n_in_j\right)$$

[note the close similarity between Eq. (6) and the matrix elements in Eqs. (2) and (3)]. It is trivially shown using Hamilton's equations, that there are two simple constants of the motion, which are

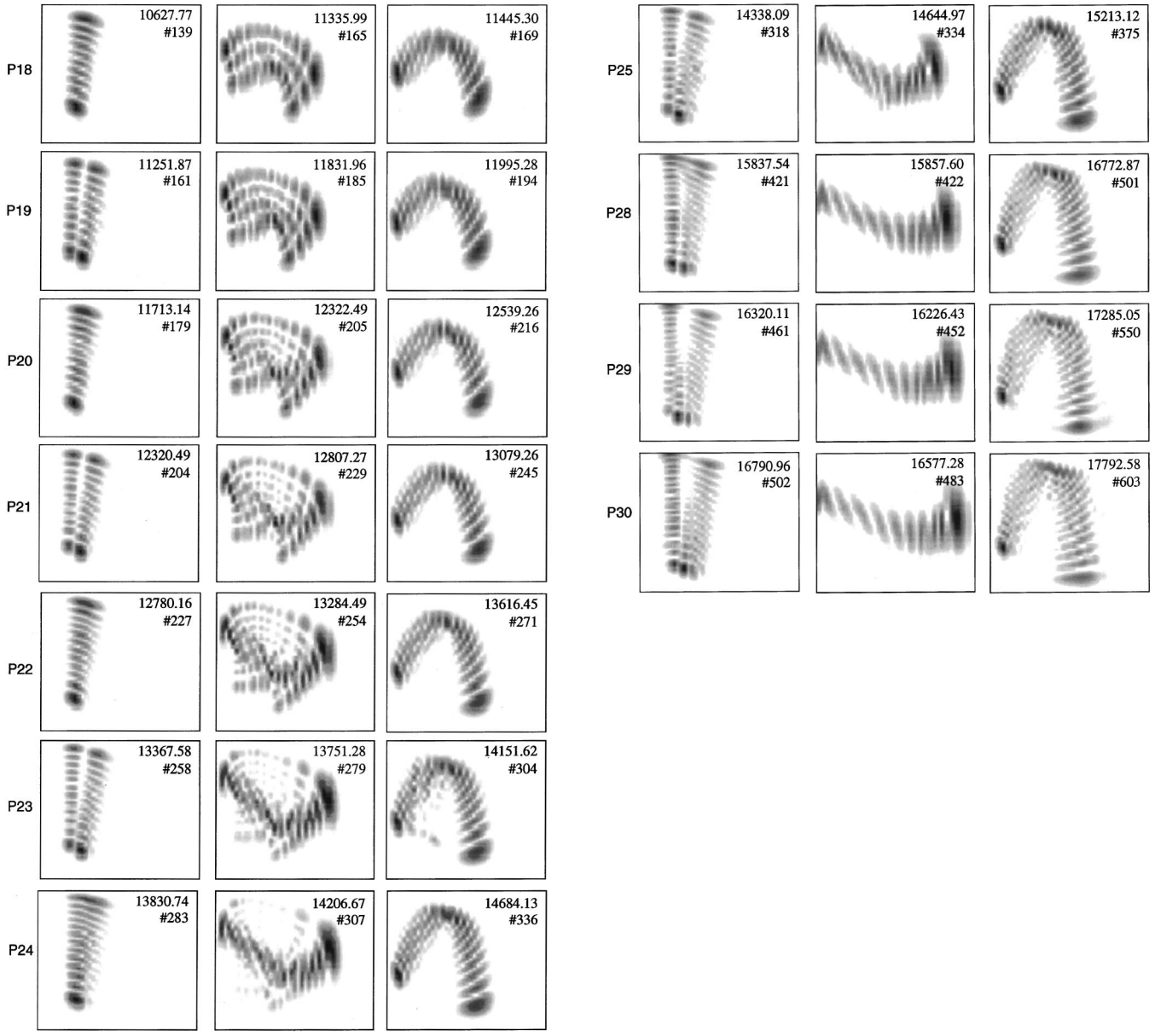

FIG. 6. Series of selected *ab initio* wave functions belonging to polyads ranging from $P=18$ to $P=30$. The coordinates and scales are the same as in Figs. 2–4. The left, middle, and right columns correspond, respectively, to the [B], [R2] and [R] periodic orbits. Note that, when P is odd, the lowest level has one quanta in OCl stretch because $P=2v_2+v_3$. All the polyads are shown between $P=18$ and $P=25$ in order to emphasize the smooth apparition of a new kind of wave functions which converge to an almost pure O–Cl stretch wave functions (middle column). This family of wave functions is scattered within each polyad. In parallel, the highest member (the right column) of each polyad, which is associated with the [R] periodic orbit (see the text, Sec. V), evolves from a pure OCl stretch to a ''horse shoe'' shape. Similarly, (the left column) the bending mode (with one quanta in OCl when P is odd) is replaced above $P=28$ by a new V-shaped family of wave functions associated with the new [B2] periodic orbit (see the text, Sec. V).

$$I_1=\tfrac{1}{2}(p_1^2+q_1^2),$$
$$I=2I_2+I_3=p_2^2+q_2^2+\tfrac{1}{2}(p_3^2+q_3^2). \tag{7}$$

The classical constants of motion I_1 and I are the classical counterparts of the good quantum numbers v_1 and $P=2v_2+v_3$. Therefore, like the quantum spectrum, the semiclassical one can be considered to consist of independent subspectra characterized by different values of the OH stretching quantum number v_1, and so the classical Hamiltonian will be handled as a two-dimensional Hamiltonian in coordinates 2 and 3 parameterized by the value of I_1. Furthermore, the classical study is simplified upon the use of the (I,θ) and (J,ψ) sets of conjugate variables, where

$$I=2I_2+I_3, \quad J=2I_2, \quad \theta=\varphi_3, \quad \psi=\varphi_2/2-\varphi_3. \tag{8}$$

Of interest are the periodic orbits (POs) of the 2D system, that is those classical trajectories, which exactly loop after some finite time in the (p_2,p_3,q_2,q_3) subspace. Since, according to Eqs. (5) and (8), one has

$$q_2=\sqrt{J}\cos(2\theta+2\psi), \quad p_2=-\sqrt{J}\sin(2\theta+2\psi),$$
$$q_3=\sqrt{2(I-J)}\cos(\theta), \quad p_3=-\sqrt{2(I-J)}\sin(\theta), \tag{9}$$

the POs of interest in this study match one of the two following criteria.

(a) POs might be associated to a fixed point in the (J,ψ) surface of section: J and ψ remain constant along the trajec-

tory and a loop is accordingly completed each time θ increases by 2π. These POs are simply obtained from Eq. (6) by solving $\partial H/\partial J=\partial H/\partial\psi=0$ for given values of I_1 and I.

(b) Two other POs are obtained when J is a constant equal to either 0 or I and ψ is free to vary. These two families of trajectories are, respectively, confined to the $q_2=0$ ($J=0$) and $q_3=0$ ($J=I$) axes. They correspond to the cases where no energy is put in the bending motion ($J=0$) or in the OCl stretching motion ($J=I$).

There actually exists another class of POs, known as rational tori (see, e.g., Refs. 44–47), but they play no role in the present study. A small number of POs (typically from 2 to 5) are thus found for each values of I_1 and I. For each of these POs, the ratio J/I remains constant (with a value between 0 and 1) along the trajectory and is a good indicator of the nature of the PO. Indeed, if J/I is close to zero, then I_2 is close to 0 and the PO corresponds to an almost pure OCl stretching motion. In contrast, if J/I is close to 1, then I_3 is close to zero and the PO is an almost pure bending trajectory. To complete this brief summary of classical dynamics, let us at last recall that a PO is said to be *stable* if neighboring trajectories oscillate around it and to be *unstable* if neighboring trajectories approach or move away from it exponentially. Moreover, a saddle-node (or tangent) bifurcation is a point in the (I_1,I,E) space, where a stable and an unstable PO are created or destroyed simultaneously.

In order to perform the PO analysis for HOCl, we need to know what values of I_1 and I must be assumed in the search for the POs for a given polyad $[v_1,P]$. These relations are simply obtained from the Einstein–Brillouin–Keller (EBK) quantization rules,[43] which state that the classical counterpart for each quantum state is a trajectory with integer or half-integer values of action integrals (action integrals can be understood as a linearly independent set of constant generalized momenta). It is now well recognized[44,45] that I_1 and I, in addition to being constants of the motion, are also action integrals of the system, and that the corresponding quantization rules for nondegenerate vibrations can simply be written as

$$I_1=v_1+\tfrac{1}{2},\quad I=P+\tfrac{3}{2}. \tag{10}$$

In other words, the classical POs, which are relevant for the study of the quantum polyad $[v_1,P]$, are obtained by replacing I_1 by $v_1+1/2$ and I by $P+3/2$ in Eqs. (6) and (8) and by subsequently solving $\partial H/\partial J=\partial H/\partial\psi=0$ [type (a) POs] or assuming $J=0$ or $J=I$ [type (b) POs] to obtain the energy values of the POs.

The result of the periodic orbit analysis for the polyads of HOCl with no excitation in the OH stretching degree of freedom ($v_1=0$, that is, $I_1=1/2$) is illustrated in Fig. 7. The small insert in the upper part represents the energy of the POs (relative to the quantum ground state) as a function of the action integral I in the range $0\leqslant I\leqslant 39.5$. For the sake of a simpler comparison, the horizontal axis is, however, labeled with the value of the quantum polyad number P obtained from the EBK quantization rule in Eq. (10) (in the relation $I=P+3/2$, P is then allowed to vary continuously). In the upper part of Fig. 7, the energy of the pure bending motion [the type (b) PO with $J=I$] has been subtracted from

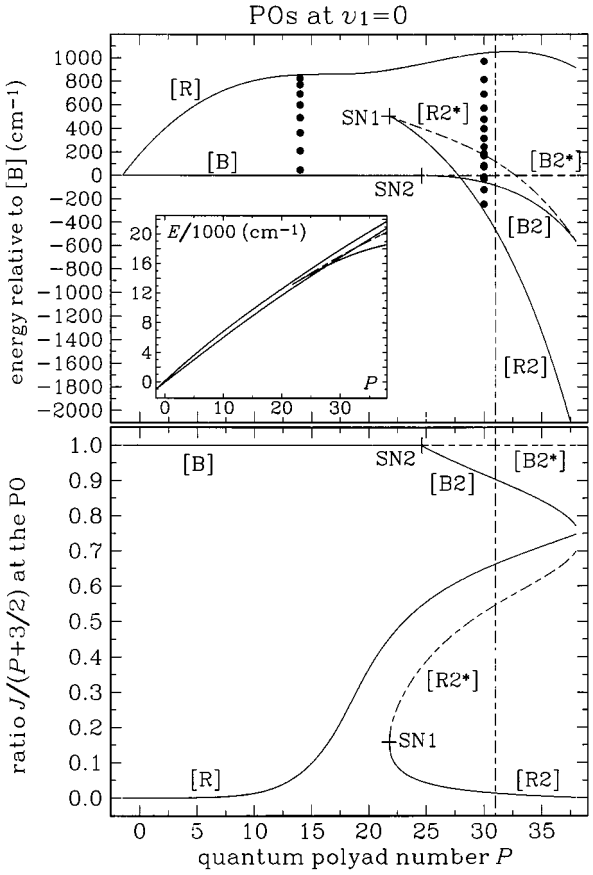

FIG. 7. The PO analysis for $v_1=0$. The upper part shows the energy of the POs as a function of P which is preferred to I ($I=P+3/2$) in order to simplify the comparison with the quantum results. The inlet shows the energy of the POs vs P, while, in the main figure, the energy of the [R] PO has been subtracted in order to magnify the evolution with P within each polyad. The POs are discussed in the text. The lower part of the figure shows the ratio J/I (or $J/(P+3/2)$) vs P. $J/I=0$ corresponds to the pure OCl stretch normal mode while $J/I=1$ corresponds to the pure bending normal mode.

all the POs, in order to magnify the interesting part of the $E(P)$ plot shown in the insert. In this plot, the vertical dashed line indicates the highest polyad with all levels taken into account in the fit ($P=31$), whereas the limit of the plot ($P=38$) is the highest polyad with at least one level taken into account in the fit. The bottom plot gives the variations of the ratio J/I as a function of P for the same POs and therefore reflects the evolution of the nature of the POs for increasing values of P.

At low energy, in the range where the Dunham expansion is a valid approximation (that is up to about polyad $P=15$), only three POs are found for each value of P. One of them, namely the type (b) PO with $J=0$ (see above), plays no role in the present study, so that only the two others, which are stable, need to be taken into account. The lowest one is labeled [B] and is simply the pure bending motion ($J=I$). The highest one is labeled [R] and is a fixed point in the (J,ψ) surface of section. The ratio J/I for [R] is equal to zero at the bottom of the well ($I=0$, that is, $P=-3/2$) and remains small in the range $0\leqslant P\leqslant 15$, so that [R] can safely be described in that range as an almost pure OCl stretching motion. The important point to realize is that the quantum levels of polyad $[v_1,P]$ always lie between the two outer-

most stable POs calculated at $I_1 = v_1 + 1/2$ and $I = P + 3/2$. In the low energy range, the lowest level in the polyad, which according to the previous section has an almost pure bending wave function, is then close to the [B] PO, whereas the highest one, with an OCl stretching wave function, lies in the vicinity of the [R] PO (see Fig. 7, where the dots represent the exact quantum levels of polyads $P = 14$ and $P = 30$). This feature is very general and the [R] and [B] POs are actually the ''necklaces'' on which the ''pearls'' of the wave functions of the lowest and highest levels are thread (this point will be illustrated in the next paragraph for polyad $P = 30$).

As P increases, [R] remains the PO with highest energy, so that the wave functions of the highest levels in the polyads are obtained by adding more and more pearls on [R]. The J/I ratio, however, increases strongly from almost zero at, say, $P = 15$ (approximately where the Dunham expansion starts to be unsatisfactory, see Sec. III) to more than 0.5 above $P = 23$, reflecting the fact that [R] avoids the dissociation pathway and acquires a marked ''horse shoe'' ($\cap$-type) shape. The conjunction of the two results—[R] remaining the highest PO throughout the spectrum and the J/I ratio increasing strongly above $P = 15$—are the classical interpretations for the series of wave functions shown in the right-hand column of Fig. 6. For the sake of illustration, in Fig. 5, the classical POs are superimposed on the quantum wave functions for the levels of the Fermi resonance Hamiltonian belonging to polyad $P = 30$: the ''horse shoe'' ($\cap$-type) shape and the necklace role of the [R] PO are very clearly seen in this figure.

In Fig. 7, the cross indicates a first saddle-node bifurcation SN1, which takes place at $P = 21.76$. Its energy relative to the quantum ground state is 13 135 cm^{-1} and the value of the momentum $J = 3.67$. Therefore, the ratio J/I at the bifurcation is small ($J/I = 0.16$) and the two POs (one stable and one unstable) created at the bifurcation have a predominant OCl stretching character. This is the reason why they are called, respectively, [R2] and [R2*]. As P further increases, the energy of the stable [R2] PO approaches that of the bending [B] PO and becomes smaller above $P = 27.8$. Therefore, for polyads $P \geqslant 28$, the quantum states are no longer located between the classical POs [B] and [R], but instead, between [R2] and [R], as can be seen in Fig. 7. Moreover, the ratio J/I decreases slowly from 0.16 to almost zero, so that the geometrical shape of [R2] almost does not change with increasing energy and [R2] is oriented along the dissociation pathway. Wave functions with pearls on this new ''necklace'' can be observed clearly for $P \geqslant 24$. At $P = 24$, the corresponding state is the fifth lowest one in the polyad. Because of the crossing of the [B] and [R2] POs (at $P = 27.8$), the wave functions with pearls along this new [R2] ''necklace'' are those of the lowest level in each polyad above $P = 28$. The occurrence of the SN1 bifurcation and the clear OCl stretch character of the stable [R2] PO born at this bifurcation are the classical interpretations for the series of wave functions shown in the middle column of Fig. 6.

On the other hand, the influence of unstable POs on quantum wave functions is much less important than the influence of stable POs. Usually, they only affect the wave functions which are energetically very close to them and, unless the quantum level and the classical unstable PO are energetically almost degenerate, the wave function is likely to appear as a mixture of several zero-order states. These are the reasons why it is not expected to observe a series of wave functions with pearls along an unstable PO. Still, it is seen in Figs. 4 and 5 that the wave function of the seventh lowest level of polyad $P = 30$ clearly stretches along [R2*], which remains close to the center of the polyad but acquires a strong bending contribution as the P quantum number increases.

A second saddle-node bifurcation, called SN2, takes place at $P = 24.50$ ($E = 14\,059\ cm^{-1}$) and $J = I = 26.00$. Note that the Fermi resonance Hamiltonian might reproduce the position of this bifurcation with an accuracy somewhat lower than for the SN1 bifurcation. Indeed, SN1 and more precisely [R2], i.e., the new stable PO born at SN1, explain the sudden increase in the energy range encompassed by a polyad, whereas SN2 is associated with more subtle details of the energy spectrum and requires a better accuracy of the fitted Hamiltonian. Up to SN2, the pure bending motion [B] characterized by $I = J$ is a stable PO in (p_2, p_3, q_2, q_3) but not a fixed point in the (J, ψ) surface of section. Above SN2, this pure bending motion is associated with a fixed point in the (J, ψ) surface of section, but this point is *unstable*, and the corresponding PO is therefore called [B2*]. A stable PO is simultaneously created at SN2 as a pure bending motion ($J/I = 1$) and is called [B2]. As P increases, J/I slowly decreases and [B2] acquires a very narrow V shape. Quantum wave functions being mostly sensitive to stable POs, the net result is that the [B] ''necklace'' with a vertical nodal structure is continuously replaced by a [B2] ''necklace'' with a more and more open V shape. The SN2 bifurcation and the replacement of [B] by [B2] are the classical interpretation for the series of quantum wave functions shown in the left-hand column of Fig. 6. The observation of this feature is made somewhat more complex by the fact that, due to the crossing of [R2] and [B2], the members of this series are the lowest level of each polyad only up to polyad $P = 29$, and then move upwards inside the polyads for $P \geqslant 30$.

All the results discussed in this section can be summarized as follows (see Fig. 6 for the wave functions).

(1) The [R] PO, associated with the highest level in each polyad, corresponds to a pure OCl stretching motion up to about $P = 15$. This family of wave functions, as well as the [R] PO, subsequently evolve progressively toward a ''horse-shoe'' type ($\cap$-type) in the same energy range where the SN1 bifurcation occurs.
(2) The SN1 bifurcation creates a new $\cup$-shaped family of wave functions, which progressively converge to a pure OCl stretching motion, thereby replacing the family of wave functions lying on top of [R].
(3) The [B] PO is associated with pure bending wave functions up to $P = 28$. The SN2 bifurcation destroys the pure bending type and creates the new V-shaped family of wave functions above $P = 28$.

VI. COMPARISON WITH EXPERIMENTAL DATA

There are 25 experimentally observed vibrational levels for HOCl. Twelve vibrational levels have been observed by

TABLE III. Comparison between experimental ($J=0$) and calculated vibrational energies and rotational constants. All the quantities are expressed in cm^{-1} and energy levels are given relative to the quantum ground state.

	Experimental			*Ab initio*		
		Rotational const			Rotational const	
(v_1,v_2,v_3)	Energy	B	$A-B$	Energy	B	$A-B$
0,0,0	0.00	0.4977	19.966[a]	0.00	0.4967	19.898
0,0,1	724.36	0.4931	19.941[b]	724.34	0.4917	19.875
0,1,0	1 238.62	0.4962	20.731[b]	1 238.62	0.4944	20.633
0,0,2	1 438.68	0.4886	19.915[c]	1 444.10	0.4868	19.852
0,2,0	2 461.21	0.4947	21.436[d]	2 456.36	0.4924	21.511
1,0,0	3 609.48	0.4973	19.171[a]	3 609.97	0.4955	19.118
0,3,0	3 668.44	0.4933	22.260[c]	3 670.39	0.4907	22.517
1,0,1	4 331.91	0.4923	19.148[e]	4 333.99	0.4903	19.106
1,1,0	4 820.43	0.4954	19.886[e]	4 821.99	0.4932	19.826
1,2,0	6 013.83	0.4940	20.762[e]	6 014.82	0.4912	20.650
2,0,0	7 049.81	0.4962	18.385[f]	7 050.41	0.4943	18.345
3,0,0	10 322.29	0.4957	17.634[e]	10 322.10	0.4935	17.538
2,2,3	11 472.47	0.4795	19.661[g]	11 493.84	0.4747	19.941
3,1,0	11 478.01	0.4940	18.223[g]	11 480.32	0.4915	18.143
2,3,3	12 590.68	0.4779	20.326[h]	12 612.66	0.4727	20.536
3,2,0	12 612.55	0.4927	18.884[i]	12 623.35	0.4873	18.918
4,0,0	13 427.39	0.4953	16.895[h]	13 425.32	0.4918	16.778
4,1,0	14 555.60	0.4937	17.465[h]	14 556.23	0.4895	17.466
4,2,1	16 352.00[j]	0.4875	18.005[h]	16 372.80	0.4823	17.877
5,0,0	16 374.00[j]	0.4949	16.168[h]	16 359.26	0.4905	16.109
6,0,0	19 124.14[k]	0.4952	15.418[l]	19 121.60	0.4892	15.355
4,4,2	19 137.29[k]	0.4799	19.250[l]	19 154.56	0.4728	19.400
5,2,1	19 243.67	0.4863	17.958[m]	19 261.38	0.4811	16.980
6,1,0	20 193.06	0.4924	16.229[m]	20 194.78	0.4870	15.670
7,0,0	21 709.07	0.4950	14.660[n]	21 716.74	0.4880	14.600

[a]Reference 7.
[b]Reference 8.
[c]Reference 9.
[d]Reference 4.
[e]Reference 8.
[f]Reference 6.
[g]Reference 12.
[h]Reference 11.
[i]Reference 10.
[j]Perturbed band origins ($J=0$, $K=0$) given in Ref. 11. The depertubed band origins are, respectively, 16 364.75 cm^{-1} for (5,0,0) and 16 362.66 cm^{-1} for (4,2,1). These two levels are strongly mixed near their band origins. The two calculated levels (fifth column) are also significantly mixed and their energies can be permuted. In contrast, the rotational constants are those of deperturbed vibrational levels (in both pairs of columns) in order to check the assignments.
[k]Perturbed band origins ($J=0$, $K=0$) to be compared with *ab initio* values in which vibrational interactions are taken into account. The deperturbed band origins are 19 126.23 and 19 135.20 cm^{-1}, respectively. These two zero-order levels are coupled by an anharmonic matrix element of 4.814 cm^{-1} (see Ref. 46).
[l]Reference 46.
[m]Reference 47.
[n]Reference 14.

absorption with a FT spectrometer up to 10 300 cm^{-1},[5–9] eight levels have been observed by Intra-Cavity Laser Absorption (ICLAS),[10–12] and five have been observed by double resonance pumping leading to the dissociation into OH+Cl, the OH product being detected by laser-induced fluorescence (LIF).[13–15,46,47] Table III gives a comparison between the experimental and the calculated vibrational energies and rotational constants. The comparison between predicted and observed vibrational energies and rotational constants enables a secure (v_1,v_2,v_3) vibrational assignment. For oscillator strength and Franck–Condon reasons, all the observed levels have only few quanta in the bending and the OCl stretch modes. Consequently these observed levels are not sensitive to the Fermi interaction discussed in Sec. IV and can be assigned with three v_i quantum numbers. The calculated rotational constants have been obtained for low energy levels by a direct energy calculation for various J (and K) values and, at higher energy, by extrapolation of the vibrational dependence observed at low energy (see below). The direct calculation is reliable up to typically 12 000–14 000 cm^{-1} because, at higher energies, there are too many rovibrational perturbations. About 100 A and 130 B values have been securely determined for *ab initio* vibrational levels assigned with three v_i quantum numbers. A fit of these rotational constants allows a determination of the vibrational dependence, and then to predict the rotational constants of

higher vibrational levels. The α and γ parameters are not significantly different from those given in Table IV of Ref. 8, except that we determined approximately $\gamma_{22}^{A} = +0.06\,\mathrm{cm}^{-1}$. The rotational constants thus obtained are reported in Table III. It should be noted that the calculated constants are almost systematically lower than the experimental values by typically 0.3% at low energy and up to 1.5% close to dissociation. The reasonable agreement between the predicted and measured rotational constants confirms the validity of the vibrational assignment of experimental levels. It should be noted that the other levels calculated in the vicinity of each observed levels have calculated rotational constants which differ significantly from the measured ones.

Several ''local'' anharmonic resonances have been inferred from the analysis of the experimental spectra for nonzero values of the total angular momentum, J and K. Indeed, the (3,1,0) level was found to interact with the (2,2,3) level via a fifth-order Fermi interaction ($\Delta v = 5$) with a matrix element of 0.51 cm^{-1},[12] for $K=2$ and 3. The corresponding anharmonic operator can be $q_1 q_2 q_3^2$. Similarly, for $J=11$, $K=4$, the level (3,2,0) interacts with the level (2,3,3) via the same fifth-order interaction but the matrix element was not given.[12] Moreover, around 16 360 cm^{-1} the level (5,0,0) interacts with the level (4,2,1) via a fourth-order anharmonic interaction[11] for $K=1$. The matrix element of 13.2 cm^{-1} should correspond to the $q_1 q_2^2 q_3$ operator. Last, the level (6,0,0) interacts with the level (4,4,2) with an anharmonic matrix element of about 5 cm^{-1}. This interaction can be interpreted either as a second-order interaction [stepwise via the (5,2,1) level] due to the $q_1 q_2^2 q_3$ operator or a first order interaction of order eight ($\Delta v = 8$). As noted these anharmonic interactions occur for nonzero J and K, because, for these values the energy gap becomes comparable to the anharmonic matrix element. These anharmonic interactions have been found not to be significant for $J=0$, both in the *ab initio* and Fermi-resonant wave functions. However, in recent work, involving a collaboration with Chen and Guo some of these interactions are found for $J>0$.[48] These interactions do not occur at exactly the same values of J and K as seen experimentally, due to slight inaccuracies in the potential energy surface.

VII. CONCLUSION AND PERSPECTIVES

We have successfully analyzed the complete set of vibrational levels of HOCl almost up to (and partially above) the HOC1 dissociation channel into OH+Cl located at 19 290 cm^{-1}. This has been possible in part because of the relative simplicity of the vibrational motions in this molecule. We now have a reliable, analytical description of part of the PES of HOCl, which enables the interpretation of the dynamical properties up to about 98% of the dissociation energy. However, this analytical effective Hamiltonian is *a priori* unable to describe the photodissociation dynamics because it does not have the correct asymptotic behavior. It should also be noted that these results deal only with rotationless levels while room temperature experiments are concerned with J values up to 30 and K values ranging from 0 to 5. Moreover, it is pointed out that, close to the dissociation threshold, the accuracy of the *ab initio* vibrational energies ranges from a few cm^{-1} for the levels with most of their energy in the OH stretch to a few tens of cm^{-1} for the others levels, i.e., several orders of magnitude less than required for a quantitative comparison with the results of eigenstate resolved experiments (which are typically accurate to within 0.1 cm^{-1}). In contrast, the average properties and the width of distributions can reasonably be predicted from *ab initio* calculations.[16,17]

The analysis of the HOCl vibrations of relevance to the simple OCl bond cleavage indicates mildly coupled motion, with, however, significant manifestations of Fermi resonances. While this has made the present analysis fairly easy, it should be noted that it has also made the calculation of the very narrow resonance widths very demanding.[16,20] Further studies on the new potential, which contains the HClO isomer, are under way and the characterization of these isomerization states may present greater challenges for an effective Hamiltonian.

ACKNOWLEDGMENTS

We thank Professor Tom Rizzo, Dr. Mike Wedlock, Dr. Andrea Callegari, Julia Rebstein, and Professor J. Koput who contributed to initiate this study and for stimulating discussions. The Grenoble High Magnetic Field Laboratory is ''Laboratoire conventionné aux universités UJF et INP de Grenoble.'' SK and JMB thank the Department of Energy for financial support and JMB thanks the National Science Foundation for partial support of computational facilities.

[1] R. P. Wayne, *Chemistry of Atmospheres*, 2nd ed. (Oxford University Press, New York, 1991).
[2] J. B. Burkholder, J. Geophys. Res. **98**, 2963 (1993).
[3] L. T. Molina and M. J. Molina, J. Phys. Chem. **82**, 2410 (1978).
[4] C. M. Deely and I. M. Mills, J. Mol. Spectrosc. **114**, 368 (1985).
[5] W. J. Lafferty and W. B. Olson, J. Mol. Spectrosc. **120**, 359 (1986).
[6] F. Cavazza, G. Di Lonardo, R. Escribano, L. Fusina, P. C. Gomez, and J. Ortigoso, J. Mol. Spectrosc. **159**, 395 (1993).
[7] M. L. Juntilla, W. J. Lafferty, and J. B. Burkholder, J. Mol. Spectrosc. **164**, 583 (1994).
[8] F. Azzolini, F. Cavazza, G. Crovetti, G. Di Lonardo, R. Frulla, R. Escribano, and L. Fusina, J. Mol. Spectrosc. **168**, 494 (1994).
[9] J. M. Flaud, M. Birk, G. Wagner, J. Orphal, S. Klee, and W. J. Lafferty J. Mol. Spectrosc. **191**, 362 (1997).
[10] B. Abel, H. H. Hamann, A. A. Kachanov, and J. Troe, J. Chem. Phys. **104**, 3189 (1996).
[11] H. H. Hamann, A. Charvat, B. Abel, S. A. Kovalenko, and A. A. Kachanov, J. Chem. Phys. **106**, 3103 (1997).
[12] A. Charvat, S. F. Deppe, H. H. Hamann, and B. Abel, J. Mol. Spectrosc. **185**, 336 (1997).
[13] R. J. Barnes, G. Dutton, and A. Sinha, J. Phys. Chem. A **101**, 8374 (1997).
[14] R. J. Barnes and A. Sinha, J. Chem. Phys. **107**, 3730 (1997).
[15] M. R. Wedlock, R. Jost, and T. R. Rizzo, J. Chem. Phys. **107**, 10344 (1997).
[16] S. Skokov, J. M. Bowman, and V. A. Mandelshtam, Phys. Chem. Chem. Phys. **1**, 1279 (1999).
[17] J. Hauschildt, J. Weiss, C. Beck, S. Yu. Grebenshchikov, R. Duren, R. Schinke, and J. Koput, Chem Phys. Lett. (in press).
[18] S. Skokov, J. M. Bowman, and K. A. Peterson, J. Chem. Phys. **109**, 2662 (1998).
[19] S. Skokov, J. Qi, J. M. Bowman, C.-Y. Yang, S. K. Gray, K. A. Peterson, and V. A. Mandelshtam, J. Chem. Phys. **109**, 10273 (1998).
[20] S. Skokov and J. M. Bowman, J. Chem. Phys. (in press).
[21] M. C. Gutzwiller, J. Math. Phys. **8**, 1979 (1967).
[22] M. C. Gutzwiller, J. Math. Phys. **12**, 343 (1971).

[23] M. C. Gutzwiller, *Chaos in Classical and Quantum Mechanics* (Springer, Berlin, 1990).
[24] E. J. Heller, Phys. Rev. Lett. **53**, 1515 (1984).
[25] P. O'Connor, J. Gehlen, and E. J. Heller, Phys. Rev. Lett. **58**, 1296 (1987).
[26] J. M. G. Llorente and E. Pollak, Annu. Rev. Phys. Chem. **43**, 91 (1992).
[27] H. S. Taylor, in *Molecular Dynamics and Spectroscopy by Stimulated Emission Pumping*, edited by H.-L. Dai and R. W. Field (World Scientific, Singapore, 1995), p. 891.
[28] R. Schinke, *Photodissociation Dynamics* (Cambridge University Press, Cambridge, 1993).
[29] S. C. Farantos, Int. Rev. Phys. Chem. **15**, 345 (1996).
[30] S. C. Farantos, H. M. Keller, R. Schinke, K. Yamashita, and K. Morokuma, J. Chem. Phys. **104**, 10055 (1996).
[31] C. Beck, H. M. Keller, S. Yu. Grebenshchikov, R. Schinke, S. C. Farantos, K. Yamashita, and K. Morokuma, J. Chem. Phys. **107**, 9818 (1997).
[32] M. Joyeux, S. Yu. Grebenshchikov, and R. Schinke, J. Chem. Phys. **109**, 8342 (1998).
[33] H. Ishikawa, R. W. Field, S. C. Farantos, M. Joyeux, J. Koput, C. Beck, and R. Schinke, Annu. Rev. Phys. Chem. (in press).
[34] T. H. Dunning, Jr., J. Chem. Phys. **90**, 1007 (1989).
[35] R. A. Kendall, T. H. Dunning, Jr., and R. A. Harrison, J. Chem. Phys. **96**, 6796 (1992).
[36] H.-J. Werner and P. J. Knowles, J. Chem. Phys. **89**, 5803 (1988).
[37] P. J. Knowles and H.-J. Werner, Chem. Phys. Lett. **145**, 514 (1988).
[38] M. Joyeux, J. Chem. Phys. **109**, 2111 (1998).
[39] K. A. Peterson, S. Skokov, and J. M. Bowman (unpublished).
[40] M. V. Berry and M. Tabor, Proc. R. Soc. London, Ser. A **349**, 101 (1976).
[41] M. Joyeux, Chem. Phys. Lett. **247**, 454 (1995).
[42] M. Joyeux and L. Michaille, ACH-Models Chem. **134**, 573 (1997).
[43] V. P. Maslov and M. V. Fedoriuk, *Semiclassical Approximations in Quantum Mechanics* (Reidel, Dordrecht, 1981).
[44] M. Joyeux, Chem. Phys. **185**, 263 (1994).
[45] M. Joyeux, Chem. Phys. **203**, 281 (1996).
[46] A. Callegari, J. Rebstein, J. Muenter, R. Jost, and Tom Rizzo, J. Chem. Phys. (submitted).
[47] J. Rebstein (private communication).
[48] R. Chen, H. Guo, S. Skokov, and J. M. Bowman (unpublished).